Frontiers in Bioscience Landmark

Front. Biosci. (Landmark Ed) **2026**; 31(9): 54657
https://doi.org/10.31083/FBL54657

Original Research

Ergothioneine Attenuates Ovariectomy-Induced Bone Loss in Association With Reduced Oxidative Stress and Enhanced Type H Vessel-Related Angiogenesis

Xinping Wang[1,2], Yuanzhang Xiao[1,2], Renwei Liu[1,2], Yingchao Cai[1,2], Wuyang Liu[1], Kai Zhao[1,2,*]

[1]Department of Orthopaedics, The First Affiliated Hospital of Gannan Medical University, 341000 Ganzhou, Jiangxi, China
[2]First Clinical Medical College, Gannan Medical University, 341000 Ganzhou, Jiangxi, China
*Correspondence: crazy_kai@163.com (Kai Zhao)
Academic Editor: Viviana di Giacomo
Submitted: 7 June 2026 Revised: 10 August 2026 Accepted: 14 August 2026 Published: 15 September 2026

Abstract

Background: Ergothioneine (EGT) has been reported to alleviate estrogen deficiency-induced osteoporosis, but whether this protection is accompanied by alterations in the bone microvasculature accompany this protection remain unknown. Therefore, this study aimed to examine the effects of EGT in ovariectomized (OVX) mice, with particular attention to type H vessels. **Methods:** A total of 18 female C57BL/6J mice were randomly assigned to the sham, OVX, and OVX + EGT groups (n = 6 each). EGT was initiated 24 h after OVX and administered for 12 weeks. Femoral structure was evaluated using micro-computed tomography, hematoxylin and eosin staining, immunohistochemistry, and immunofluorescence. Meanwhile, serum assays were used to characterize bone turnover and oxidative stress. In addition, mouse bone-derived type H endothelial cells were exposed to EGT. The localization of organic cation transporter novel type 1 (OCTN1) was examined by immunofluorescence. Angiogenic activity was measured in Matrigel, while OCTN1 gene and protein expression were assessed by reverse-transcription quantitative polymerase chain reaction and Western blotting, respectively. **Results:** In OVX mice, EGT increased bone mineral density and improved trabecular microarchitecture. Serum superoxide dismutase activity and glutathione concentrations were higher after EGT administration, whereas advanced oxidation protein products and malondialdehyde levels were lower. Bone sections also showed a larger $CD31^+$ vascular area, more osterix-positive (Osx^+) osteogenic cells, and a closer spatial association between these signals. EGT increased OCTN1 expression *in vitro* and promoted angiogenesis. **Conclusions:** Early administration of EGT alleviated OVX-induced bone loss. This effect may be linked to reduced oxidative stress and enhanced angiogenesis related to type H vessels.

Keywords: angiogenesis; ergothioneine; osteoporosis; ovariectomy; oxidative stress; postmenopausal

1. Introduction

Postmenopausal osteoporosis (PMOP) involves progressive loss of bone mass and disruption of bone microarchitecture, changes that compromise skeletal strength and increase susceptibility to fracture [1,2]. In China, osteoporosis affects more than 30% of postmenopausal women following the marked decline in estrogen after menopause [3]. The lifetime probability of an osteoporotic fracture among people aged 50 years or older is approximately one in three for women and one in five for men [4]. Population aging is expected to further amplify the clinical and economic consequences of these fractures [5]. Although PMOP has a multifactorial origin, estrogen deficiency remains one of its principal drivers [6], and the oxidative imbalance associated with estrogen loss is considered an important component of disease development [7].

Oxidative stress develops when oxidant generation outstrips antioxidant capacity, allowing reactive oxygen species (ROS), reactive nitrogen species, and other free radicals to accumulate [8,9]. Persistent redox imbalance can then injure cells and tissues [10]. Within bone, this disturbance of metabolic homeostasis has been linked to reduced bone mineral density (BMD) [11]. It favors osteoclastogenesis by increasing receptor activator of nuclear factor-κB ligand (RANKL) expression and increasing the ratio of RANKL to osteoprotegerin [12,13]. Oxidative stress also impairs the commitment of bone progenitors to the osteoblast lineage and diminishes osteoblast activity [14], while promoting apoptosis of osteoblasts and osteocytes [15,16]. Type H vessels are a specialized subset of bone capillaries that contribute to skeletal homeostasis by linking angiogenesis to osteogenesis [17,18]. Their decline under oxidative conditions has been implicated in bone loss [19,20], suggesting that preservation of type H vessel-related angiogenesis may offer a potential strategy for limiting PMOP.

Ergothioneine (EGT) is a naturally occurring, sulfur-containing, non-proteinogenic amino acid with antioxidant and anti-inflammatory activity [21,22]. It is biosynthesized mainly by fungi, algae, and certain bacteria and oc-

curs predominantly as interconvertible thiol and thione tautomers [23]. Because EGT preferentially accumulates in tissues susceptible to oxidative injury, it has attracted interest as a potential intervention for disorders driven by oxidative stress [24,25]. Guo et al. [26] showed that EGT upregulated heme oxygenase-1 (HO-1) and catalase, thereby limiting RANKL-induced ROS accumulation and mitogen-activated protein kinase (MAPK) signaling to suppress osteoclast differentiation *in vitro*, and attenuated bone loss in ovariectomized (OVX) mice. A separate study reported that EGT given early after OVX decreased mitochondrial ROS, inhibited nuclear factor-κB (NF-κB)/nuclear factor of activated T cells 1 (NFATc1) signaling, and attenuated both osteoclastogenesis and bone loss [27]. These investigations concentrated on osteoclast-mediated effects and did not evaluate the bone microvasculature; consequently, it remains uncertain whether EGT is associated with changes in type H vessels.

Using a bilateral OVX mouse model, we examined EGT in relation to bone loss and systemic oxidative stress. We quantified $CD31^+$ vascular area, osterix-positive (Osx^+) osteogenic cells, and their spatial proximity in bone and assessed organic cation transporter novel type 1 (OCTN1) expression and angiogenic activity after EGT exposure in bone-derived type H endothelial cells.

2. Materials and Methods

2.1 Animal Studies

Twenty-four female C57BL/6J mice, 8 weeks of age and weighing 20 ± 2 g, were supplied by the Gannan Institute of Innovation and Translational Medicine. The *in vivo* study used 18 animals; the other six received no intervention and were used exclusively as donors of primary bone-derived type H endothelial cells. The *in vivo* sample size was selected based on comparable OVX studies and the reduction principle of the 3Rs. All procedures involving animals were authorized by the Experimental Animal Care and Use Committee of the First Affiliated Hospital of Gannan Medical University (No. GMU2022126). Animal care and experimentation complied with the National Institutes of Health Guide for the Care and Use of Laboratory Animals, and the study followed the ARRIVE guidelines. Animals were maintained in a specific pathogen-free facility under a 12-h light/12-h dark schedule at 22 ± 2 °C and 50 ± 10% relative humidity, with unrestricted access to chow and water. After 1 week of acclimatization, each of the 18 animals assigned to the *in vivo* experiment received a unique identifier. A computer-generated random sequence was then used to distribute them equally among the Sham, OVX, and OVX + EGT groups (six animals per group). Starting 24 h after the operation, saline was given by oral gavage once daily to the Sham and OVX groups. The OVX + EGT group was gavaged on the same schedule with EGT at 70 mg/kg/day for 12 weeks (EGT dissolved in saline; L864254-5g, Shanghai Macklin Biochemical Co., Ltd., Shanghai, China). The selected dose and oral route were based on established protocols [28].

Bilateral ovariectomy was carried out with reference to previously reported procedures [29,30]. Anesthesia was induced by intraperitoneal administration of 1% pentobarbital sodium at 40 mg/kg (P3761, Sigma-Aldrich, St. Louis, MO, USA). Under aseptic conditions, hair was removed from the dorsal lumbar area and the skin was disinfected. A midline skin incision of approximately 1 cm was created over the lumbar spine, and the peritoneal cavity was approached through an incision in the paravertebral muscles on each side. The ovary, adjacent oviduct, and surrounding fat pad were gently brought outside the abdominal cavity. After ligation of the utero-ovarian vascular pedicle, the ovary was removed; this procedure was repeated contralaterally. Muscle and skin were closed in separate layers. Sham-operated animals underwent identical surgical exposure, but their ovaries were neither ligated nor excised. For the first 3 postoperative days, every mouse received intraperitoneal penicillin G sodium (50 mg/kg; PHR2642, Sigma-Aldrich, St. Louis, MO, USA) as antimicrobial prophylaxis and subcutaneous meloxicam (2 mg/kg; PHR1799, Sigma-Aldrich, St. Louis, MO, USA) for pain control. Oral gavage commenced 24 h after surgery and continued for the 12-week study period. At study completion, blood was obtained by cardiac puncture under deep anesthesia, immediately before euthanasia. The animals were subsequently euthanized by CO_2 inhalation, after which the femurs were collected. Whole blood was kept at room temperature for 30 min to permit clotting and was centrifuged at 3000 ×g for 10 min at 4 °C. Serum was removed, divided into aliquots, and stored at −80 °C without repeated freeze-thawing until biochemical testing.

2.2 Cell Culture

Primary bone-derived type H endothelial cells were obtained from the six untreated 8-week-old female C57BL/6J donor mice. Three biologically independent isolations were conducted, and each isolation used pooled marrow from two donors.

Femurs and tibiae were removed bilaterally under aseptic conditions and cleared of adherent soft tissue. Following excision of both epiphyses, each bone was positioned with its cut surface directed downward in a perforated 0.5-mL tube placed inside a 1.5-mL collection tube. Centrifugation at 10,000 ×g for 15 s at room temperature expelled the marrow into the outer tube. The recovered marrow was suspended in phosphate-buffered saline (PBS) containing 2% fetal bovine serum, filtered through a 70-μm mesh, and pelleted at 300 ×g for 10 min. Cells were plated at 1×10^6 cells per 100-mm dish. For the initial 24 h, cultures were maintained in Dulbecco's modified Eagle's medium containing 10% fetal bovine serum and 1% penicillin-streptomycin (all from Gibco, Thermo Fisher Scientific, Grand Island, NY, USA). Incubation was

performed at 37 °C in humidified 5% CO_2. The cultures were then switched to endothelial cell medium (1001, ScienCell Research Laboratories, Carlsbad, CA, USA) and maintained for a further 5–7 days; fresh medium was supplied every 2–3 days.

For fluorescence-activated cell sorting, adherent cells were released with Accutase for 2 min at 37 °C (00-4555-56, Thermo Fisher Scientific, Waltham, MA, USA). The resulting suspension was stained for 1 h at 4 °C with PE-labeled anti-Ter119 (E-AB-F1125D, Elabscience Biotechnology Inc., Wuhan, Hubei, China), APC/Cy7-labeled anti-CD45 (103116, BioLegend, San Diego, CA, USA), Alexa Fluor 488-labeled anti-EMCN (53-5851-82, Invitrogen, Thermo Fisher Scientific, Carlsbad, CA, USA), and Alexa Fluor 647-labeled anti-CD31 (102516, BioLegend, San Diego, CA, USA). Forward- and side-scatter parameters were first used to remove debris and doublets. $CD45^+$ and $Ter119^+$ events were subsequently excluded, and $CD31^+EMCN^+$ cells in the remaining $CD45^-Ter119^-$ fraction were collected as bone-derived type H endothelial cells on a FACSAria instrument (BD Biosciences, San Jose, CA, USA). FACSDiva version 6.1.3 (BD Biosciences) was used to process the cytometry data.

When cultures reached 70–80% confluence, the cells generated by each independent isolation were assigned separately to Control, Vehicle, or EGT conditions. Selection of the test concentration was informed by an earlier endothelial-cell study in which 0.1–0.3 mM EGT produced biological activity without detectable cytotoxicity [31]. Cells in the EGT condition therefore received 50 µg/mL EGT (approximately 0.22 mM) for 24 h. An equal volume of the sterile saline used to dissolve EGT was added to Vehicle cultures, whereas no supplement was added to Control cultures. Cells were collected after these interventions for the analyses described below.

2.3 Micro-Computed Tomography (Micro-CT)

Excised femurs were preserved in 75% ethanol and examined with a high-resolution µCT 80 scanner (SCANCO Medical AG, Brüttisellen, Switzerland). Trabecular bone in the distal femoral metaphysis was acquired at a 12-µm isotropic voxel resolution, using 55 kV and an integration time of 145 ms. The analysis volume consisted of 300 consecutive slices extending proximally from the distal femoral growth plate. After reconstruction, CTAn version 1.18 (Bruker microCT N.V., Kontich, Belgium) was used to derive bone mineral density (BMD), bone volume fraction (BV/TV), trabecular thickness (Tb.Th), trabecular number (Tb.N), and trabecular separation (Tb.Sp). Image collection, delineation of the trabecular region of interest, and reporting of microarchitectural outcomes followed previously published methods [19].

2.4 Enzyme-Linked Immunosorbent Assay

Bone-turnover indices and vascular endothelial growth factor (VEGF) were quantified in serum using commercial enzyme-linked immunosorbent assay kits. The assays were completed as directed by the manufacturer. Optical density was recorded at 450 nm with a Multiskan FC microplate photometer (Thermo Fisher Scientific Oy, Vantaa, Finland), and the relevant calibration curve was used to determine each concentration. The panel comprised total osteocalcin (OCN, ml063317, Shanghai Enzyme-linked Biotechnology Co., Ltd., Shanghai, China), procollagen type I N-terminal propeptide (P1NP, ml063063, Shanghai Enzyme-linked Biotechnology Co., Ltd., Shanghai, China), alkaline phosphatase (ALP, ml002235, Shanghai Enzyme-linked Biotechnology Co., Ltd., Shanghai, China), tartrate-resistant acid phosphatase (TRAP, ml058339, Shanghai Enzyme-linked Biotechnology Co., Ltd., Shanghai, China), C-terminal telopeptide of type I collagen (CTX-1, ml002265, Shanghai Enzyme-linked Biotechnology Co., Ltd., Shanghai, China), N-terminal telopeptide of type I collagen (NTX, ml002102, Shanghai Enzyme-linked Biotechnology Co., Ltd., Shanghai, China), and VEGF (ml106702, Shanghai Enzyme-linked Biotechnology Co., Ltd., Shanghai, China).

2.5 Measurement of Oxidative Stress Markers

Commercial assay kits were used to determine serum superoxide dismutase activity (SOD, KTB1030, Abbkine Scientific Co., Ltd., Wuhan, Hubei, China) and the concentrations of reduced glutathione (GSH, KTB1600, Abbkine Scientific Co., Ltd., Wuhan, Hubei, China), advanced oxidation protein products (AOPPs, KTB1060, Abbkine Scientific Co., Ltd., Wuhan, Hubei, China), and malondialdehyde (MDA, KTB1050, Abbkine Scientific Co., Ltd., Wuhan, Hubei, China). All measurements were performed according to the manufacturer's instructions.

2.6 Hematoxylin and Eosin (H&E) Staining

For H&E staining and OCN immunohistochemistry, three of the six mice in each experimental group were randomly selected using a random-number generator. Femoral specimens from these mice were immersed in 4% paraformaldehyde (pH 7.0) for 48 h and then decalcified at 4 °C in 10% ethylenediaminetetraacetic acid (EDTA; pH 7.4). The EDTA solution was renewed at 3-day intervals. After approximately 2 weeks, completion of decalcification was verified by needle penetration. Samples were processed sequentially through 75%, 80%, 90%, 95%, and 100% ethanol, cleared with xylene, and embedded in paraffin. Serial 5-µm coronal sections were cut to provide complete cross-sections of the femoral marrow cavity. After paraffin removal and rehydration, sections were exposed to hematoxylin for 5 min and differentiated in 1% acid alcohol for 30 s. They were then rinsed in running tap water for 15–30 min until blueing was complete, followed by

a 3-min eosin counterstain. Dehydrated and cleared sections were coverslipped with neutral resin. Bone morphology was evaluated by light microscopy (Nikon Corporation, Tokyo, Japan), and ImageJ (National Institutes of Health, Bethesda, MD, USA) was used to quantify the number of bone marrow adipocytes per high-power field. For each mouse, measurements from three sections were averaged to obtain a single value.

2.7 Immunohistochemistry

Following antigen retrieval and blocking, bone sections were exposed overnight at 4 °C to a rabbit anti-OCN antibody (1:100; DF12303, Affinity Biosciences, Cincinnati, OH, USA). Binding was detected by a 2-h room-temperature incubation with horseradish peroxidase (HRP)-conjugated goat anti-rabbit secondary antibody (1:200; S0001, Affinity Biosciences). A 3,3′-diaminobenzidine substrate kit (DAB; P0203, Beyotime Biotechnology, Shanghai, China) was used for color development, and hematoxylin was applied as the nuclear counterstain. After mounting in neutral resin, sections were photographed on an Axio Imager D2 bright-field microscope (Carl Zeiss Microscopy GmbH, Jena, Germany). ImageJ was used for semiquantitative assessment, expressed as the mean optical density of OCN-positive staining. Measurements from three sections were averaged to obtain a single value per mouse.

2.8 Immunofluorescence

For cellular immunofluorescence, type H endothelial cells were grown on coverslips at 37 °C in humidified 5% CO_2 until approximately 80% confluent. Cultures were washed three times with ice-cold PBS, fixed in 4% paraformaldehyde for 20 min at room temperature, and permeabilized for 15 min with 0.1% Triton X-100 in PBS. Nonspecific binding was blocked with 5% bovine serum albumin for 1 h at room temperature. In a humidified chamber at 4 °C, cells were incubated overnight with a mouse polyclonal anti-OCTN1 antibody (1:700; H00006583-A01, Novus Biologicals, Centennial, CO, USA) together with an Alexa Fluor 488-conjugated anti-CD31 antibody (1:200; FAB3628G, R&D Systems, Minneapolis, MN, USA). After PBS washing, Alexa Fluor 594-conjugated goat anti-mouse IgG (1:500; ab150116, Abcam, Cambridge, UK) was applied for 1 h at room temperature in the dark. Nuclei were labeled with 4′,6-diamidino-2-phenylindole (DAPI, 1 µg/mL, 5 min), and coverslips were secured with antifade mounting medium.

A separate preparation was used for immunofluorescence of bone tissue. Femurs were fixed for 4 h at 4 °C in 4% paraformaldehyde and decalcified for 14 days at 4 °C with 0.5 M EDTA (pH 7.4). After the femurs were embedded in optimal cutting temperature compound and frozen overnight, serial 30-µm sections were produced on a cryostat (Leica Microsystems GmbH, Wetzlar, Germany). Sections were rinsed three times in PBS and blocked for 1 h at room temperature with 10% goat serum. Primary staining was performed overnight at 4 °C with mouse anti-CD31 (1:500; BF8133, Affinity Biosciences, Cincinnati, OH, USA) and rabbit anti-osterix (Osx; 1:200; AF7080, Affinity Biosciences). The following secondary antibodies were then applied together for 1 h at room temperature in the dark: Alexa Fluor 594-conjugated goat anti-mouse IgG (1:500; ab150116, Abcam, Cambridge, UK) and Alexa Fluor 488-conjugated goat anti-rabbit IgG (1:500; ab150077, Abcam). An Axio Imager D2 fluorescence microscope (Carl Zeiss Microscopy GmbH, Jena, Germany) was used for image acquisition. With ImageJ, $CD31^+$ vascular signals were expressed as a percentage of area and Osx^+ cells were counted.

2.9 Tube Formation Assay

The assay was performed as previously described [32]. Matrigel basement membrane matrix (356234, Corning Inc., Corning, NY, USA) was allowed to thaw at 4 °C overnight. Aliquots of 50 µL were distributed uniformly into the wells of a 96-well plate and polymerized for 30 min at 37 °C. After the specified interventions, type H endothelial cells were collected and suspended in endothelial cell medium (1001, ScienCell Research Laboratories, Carlsbad, CA, USA) containing 10% fetal bovine serum (Gibco, Thermo Fisher Scientific, Grand Island, NY, USA). Each coated well received 2×10^4 cells in 100 µL. Cultures were incubated for 6 h at 37 °C in a humidified atmosphere containing 5% CO_2. Network-like structures were viewed with an inverted phase-contrast microscope (Leica Microsystems GmbH, Wetzlar, Germany). Three to five fields were selected at random from each group, and total tube length was measured in ImageJ as the index of tube-forming activity.

2.10 Reverse-Transcription Quantitative Polymerase Chain Reaction (RT-qPCR) Analysis

RNA was purified from type H endothelial cells with the EZ-press RNA Purification Kit (B0004D, EZBioscience, Roseville, MN, USA), following the supplier's instructions. A NanoDrop spectrophotometer (Thermo Fisher Scientific, Waltham, MA, USA) was used to evaluate RNA yield and purity. For each sample, 0.5 µg RNA was converted to complementary DNA with the Color Reverse Transcription Kit (A0010CGQ, EZBioscience). RT-qPCR was conducted on a QuantStudio 5 Real-Time PCR System (Applied Biosystems, Thermo Fisher Scientific, Foster City, CA, USA) using 2× Color SYBR Green qPCR Master Mix (A0012-R1, EZBioscience). The 20-µL reactions were initiated at 95 °C for 5 min, followed by 40 cycles consisting of 95 °C for 10 s and 60 °C for 30 s. Product specificity was checked by a melting-curve analysis run from 65 °C to 95 °C. Each sample was tested in triplicate, and *GAPDH* served as the endogenous reference. Table 1 lists the primer sequences.

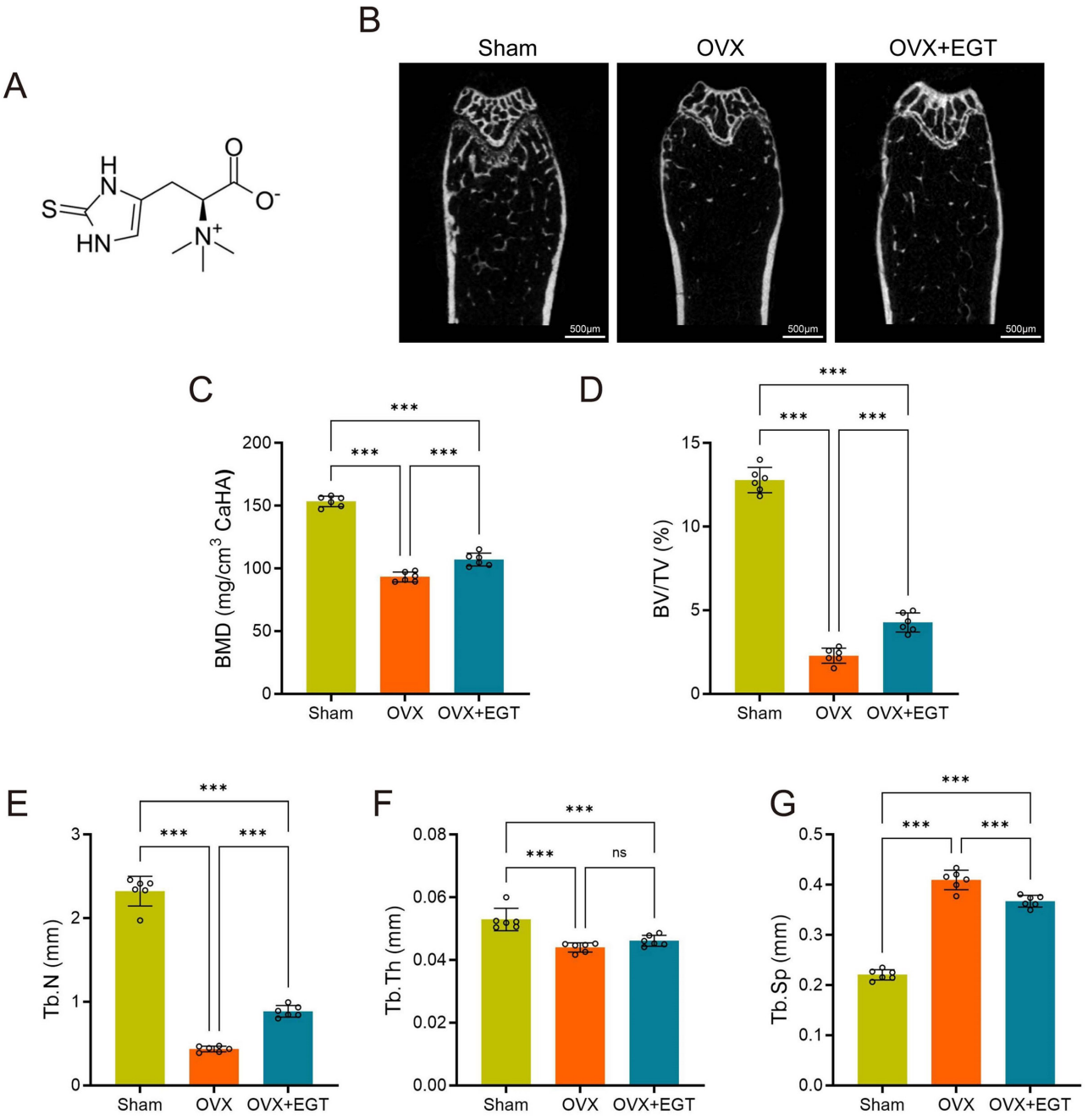

Fig. 1. EGT administration attenuates OVX-induced bone loss. (A) Chemical structure of EGT. (B) Representative micro-CT images of femoral microarchitecture from three experimental groups (Sham, OVX, and OVX + EGT); scale bar: 500 μm. (C) Bone mineral density (BMD). (D) Bone volume fraction (BV/TV). (E) Trabecular number (Tb.N). (F) Trabecular thickness (Tb.Th). (G) Trabecular separation (Tb.Sp). Data are presented as the mean ± SD (n = 6 mice per group). ***$p < 0.001$; ns, not significant. OVX, ovariectomized; EGT, ergothioneine. The figure was created using Figdraw (https://www.figdraw.com/).

2.11 Western Blot Assay

Type H endothelial cells were lysed in radioimmunoprecipitation assay (RIPA) buffer (FD008, FDbio, Hangzhou, Zhejiang, China) containing 1% (v/v) protease and phosphatase inhibitor cocktail (FD1001, FDbio). Sample preparation was conducted on ice. Total protein was quantified by the bicinchoninic acid method (BCA kit 23227, Thermo Fisher Scientific, Waltham, MA, USA). For each lane, 30 μg of protein was resolved by 10% sodium dodecyl sulfate–polyacrylamide gel electrophoresis (SDS-PAGE) and transferred to a polyvinylidene difluoride membrane (IPFL00010, MilliporeSigma, Burlington, MA, USA). Membranes were blocked in 5% non-fat milk for 1 h at room temperature. They were then incubated at

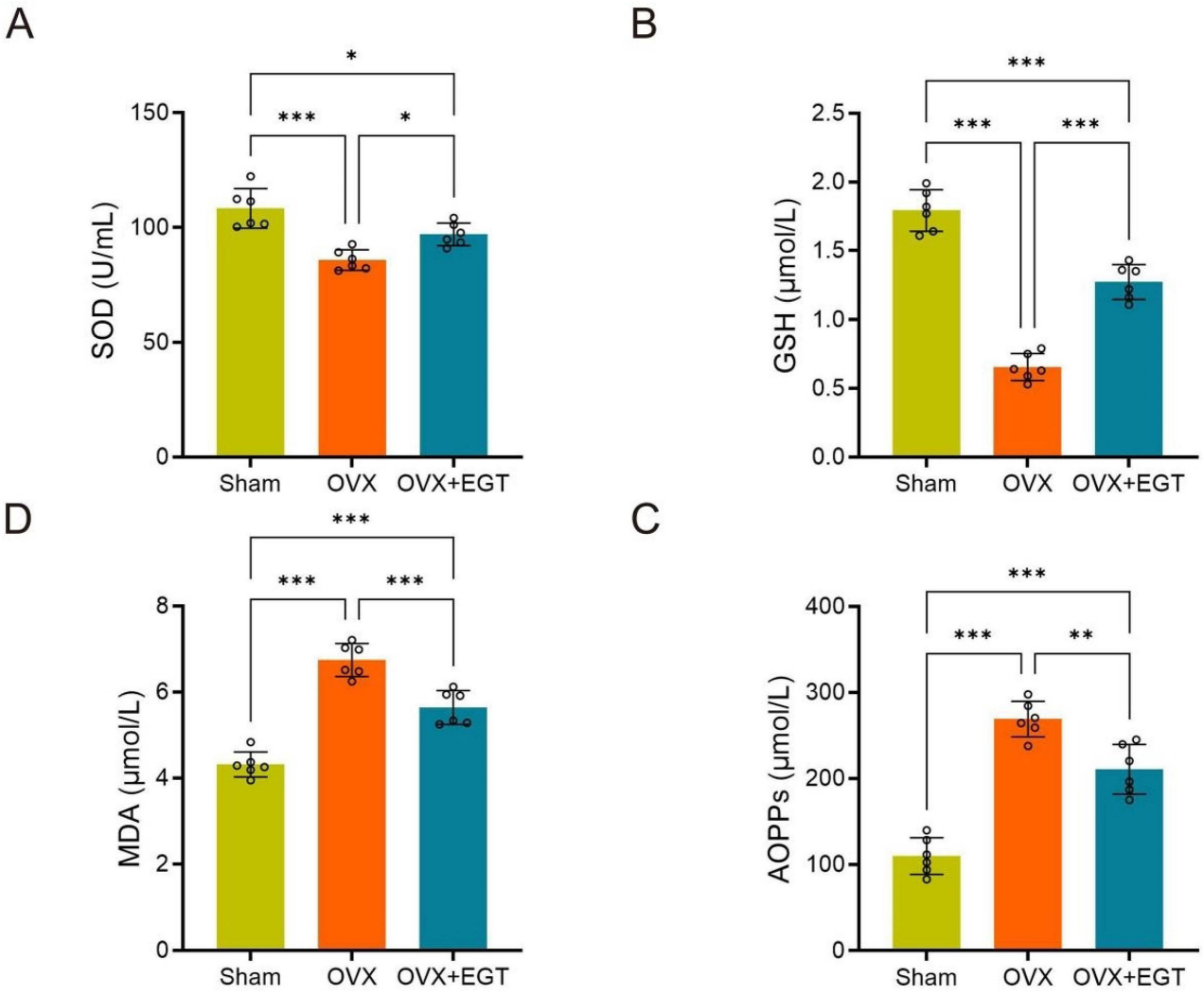

Fig. 2. EGT attenuates oxidative stress in OVX mice. (A) Superoxide dismutase (SOD). (B) Glutathione (GSH). (C) Advanced oxidation protein products (AOPPs). (D) Malondialdehyde (MDA). Data are presented as the mean ± SD (n = 6 mice per group). *p < 0.05, **p < 0.01, and ***p < 0.001. The figure was created using Figdraw (https://www.figdraw.com/).

Table 1. Primer sequences used for RT-qPCR.

Gene	Primer sequence (5′-3′)
OCTN1	Forward: 5′-GCTGGGAGTACGACAAGGAC-3′
	Reverse: 5′-GAAGAACAGGGAGGTGGTGA-3′
GAPDH	Forward: 5′-AACTTTGGCATTGTGGAAGG-3′
	Reverse: 5′-GGATGCAGGGATGATGTTCT-3′

4 °C overnight with rabbit anti-OCTN1 (1:1000; DF9724, Affinity Biosciences, Cincinnati, OH, USA) and rabbit anti-GAPDH (1:3000; AF7021, Affinity Biosciences). Following washing, HRP-conjugated goat anti-rabbit IgG (1:5000; M21003, Abmart, Shanghai, China) was applied for 1 h at room temperature. Bands were detected with enhanced chemiluminescence reagent (34577, Thermo Fisher Scientific). Band intensities from three independent experiments were quantified using ImageJ. OCTN1 band intensity was normalized to the corresponding GAPDH band intensity and expressed relative to the Control group.

2.12 Statistical Analysis

Results are reported as mean ± standard deviation (SD). Distributional normality was examined with the Shapiro-Wilk test, and equality of variances was evaluated with Levene's test. Because every dataset satisfied both assumptions, group differences were tested by one-way analysis of variance, followed by Tukey's multiple-comparison procedure. All p values were derived from two-sided tests, with $p < 0.05$ defining statistical significance. Significance levels were denoted as *p < 0.05, **p < 0.01, and ***p < 0.001; ns indicated no statistically significant difference. Analyses were performed in IBM SPSS Statistics 19.0 (IBM Corp., Armonk, NY, USA) and GraphPad Prism 9.0 (GraphPad Software, San Diego, CA, USA).

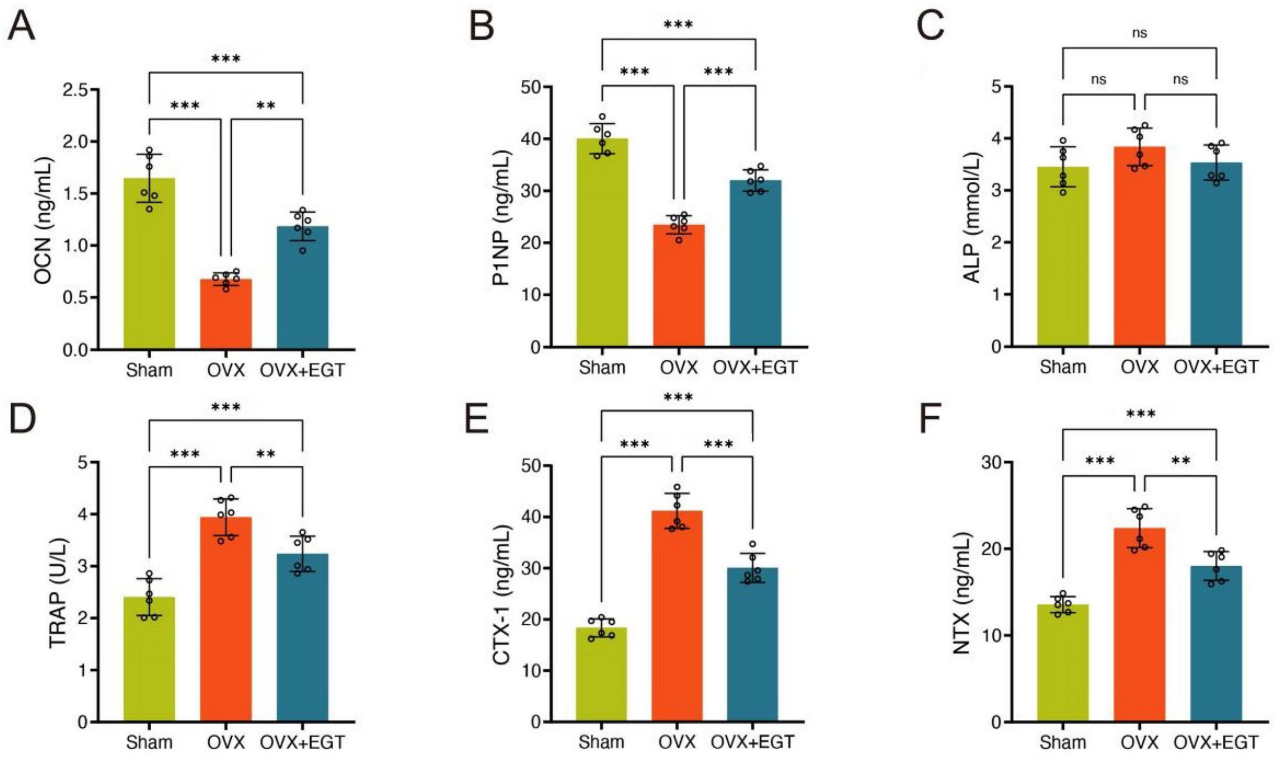

Fig. 3. Effects of EGT on serum bone turnover markers. (A) Osteocalcin (OCN). (B) Procollagen type I N-terminal propeptide (P1NP). (C) Alkaline phosphatase (ALP). (D) Tartrate-resistant acid phosphatase (TRAP). (E) C-terminal telopeptide of type I collagen (CTX-1). (F) N-terminal telopeptide of type I collagen (NTX). Data are presented as the mean ± SD (n = 6 mice per group). $^{**}p < 0.01$, $^{***}p < 0.001$; ns, not significant. The figure was created using Figdraw (https://www.figdraw.com/).

3. Results

3.1 EGT Administration Attenuates OVX-Induced Bone Loss

Femoral trabecular bone was examined by micro-CT to determine whether EGT altered the skeletal changes associated with OVX. The molecular structure of EGT is provided in Fig. 1A. Three-dimensional reconstructions showed a compact, interconnected trabecular network in Sham animals. By contrast, OVX was accompanied by fewer trabeculae and wider spaces between them, whereas the OVX + EGT group displayed a less disrupted architecture (Fig. 1B). Relative to the Sham group, OVX significantly lowered BMD and BV/TV. Both indices were higher in EGT-treated OVX mice than in untreated OVX mice (Fig. 1C,D). OVX also reduced Tb.N and increased Tb.Sp; EGT shifted both measures in the opposite direction (Fig. 1E,G). Tb.Th was numerically greater after EGT administration, but the difference between the OVX and OVX + EGT groups did not reach statistical significance (Fig. 1F).

3.2 EGT Attenuates Oxidative Stress in OVX Mice

To assess the antioxidant effects of EGT, serum antioxidant components and oxidative damage markers were measured. SOD activity and GSH concentration were lower in OVX mice than in Sham mice, while both measures were significantly higher in the OVX + EGT group than in the untreated OVX group (Fig. 2A,B). The opposite pattern was observed for indices of oxidative damage: OVX increased AOPPs and MDA, and EGT administration reduced both markers relative to OVX alone (Fig. 2C,D). Thus, early EGT exposure was accompanied by greater antioxidant capacity and lower circulating oxidative products in OVX mice.

3.3 Effects of EGT on Serum Bone Turnover Markers

Serum markers were analyzed to characterize bone turnover. OVX reduced OCN and P1NP relative to Sham, whereas both formation-related markers were significantly higher following EGT administration (Fig. 3A,B). ALP did not differ significantly among the groups (Fig. 3C). For resorption-related measures, TRAP activity and CTX-1 concentration were elevated after OVX and were lower in the OVX + EGT group (Fig. 3D,E). NTX followed the same pattern, increasing in OVX mice and decreasing after EGT intervention (Fig. 3F).

3.4 EGT Improves Osteogenic Activity in OVX Mice

Histological examination revealed numerous trabeculae and relatively few marrow adipocytes in Sham femora. OVX specimens contained less trabecular bone and

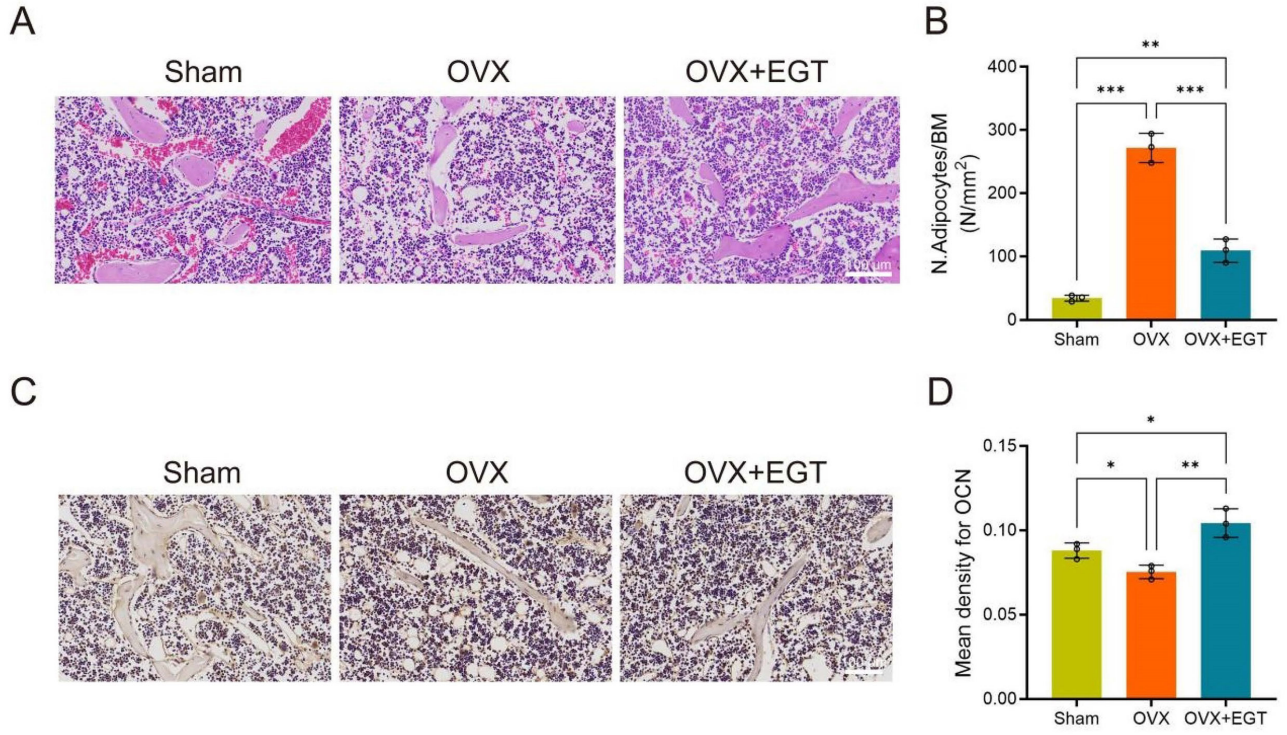

Fig. 4. EGT improves osteogenic activity in OVX mice. (A) H&E-stained bone tissue sections showing the number and area of trabeculae (pink-stained cord- or clump-like structures) and the morphological characteristics and distribution of adipocytes (vacuolated cells with clear cytoplasm); scale bar: 100 µm. (B) Quantitative analysis of adipocyte number per square millimeter of bone marrow (N.Adipocytes/BM) through cell counting of pathological images. (C) Immunohistochemical staining of bone tissue sections depicting the distribution of OCN; scale bar: 100 µm. (D) Quantitative analysis of mean optical density of OCN-positive staining by densitometric evaluation of immunohistochemical images. Data are presented as the mean ± SD (n = 3 mice per group). $*p < 0.05$, $**p < 0.01$, and $***p < 0.001$. H&E, hematoxylin and eosin. The figure was created using Figdraw (https://www.figdraw.com/).

more adipocytes, while sections from EGT-treated OVX mice showed better-preserved trabecular structure and less adipocyte accumulation (Fig. 4A). Adipocyte density was significantly greater after OVX than after Sham surgery and was lower in the OVX + EGT group than in the OVX group (Fig. 4B). OCN immunohistochemistry produced prominent positive staining in Sham bone but weaker staining after OVX (Fig. 4C). Compared with the untreated OVX group, the EGT group had a significantly greater mean optical density of OCN-positive staining (Fig. 4D).

3.5 EGT Increases CD31$^+$ Vascular Area and Osx$^+$ Osteogenic Cell Abundance and Improves Their Spatial Association in OVX Mice

Double immunofluorescence for CD31 and Osx was used to examine the spatial relationship between vascular structures and osteogenic cells in bone. Sham sections contained abundant CD31$^+$ vascular profiles with Osx$^+$ cells frequently located nearby. OVX reduced both signals and decreased the frequency of areas in which they were closely apposed. Sections from EGT-treated OVX mice showed more CD31$^+$ vascular staining, more Osx$^+$ cells, and more regions of close spatial proximity between the two signals (Fig. 5A). Quantification showed that CD31$^+$ area and Osx$^+$ cell number were significantly lower after OVX than after Sham surgery. Both measures were significantly higher in the OVX + EGT group than in the OVX group (Fig. 5B,D). Serum VEGF was likewise reduced by OVX and increased after EGT administration (Fig. 5C).

3.6 EGT Promotes Angiogenesis in Type H Endothelial Cells

Bone-derived CD31$^+$EMCN$^+$ endothelial cells were collected by fluorescence-activated cell sorting after exclusion of CD45$^+$ and Ter119$^+$ cells (Fig. 6A). In culture, the sorted cells displayed an endothelial-like appearance under bright-field microscopy (Fig. 6B). OCTN1 immunofluorescence was detected within CD31$^+$ cells, as shown by overlap between the OCTN1 and CD31 channels (Fig. 6C). Western blotting showed a stronger OCTN1 protein band in EGT-exposed cells. In addition, quantitative analysis showed that the relative protein expression of OCTN1 was significantly higher in the EGT group than in the Control and Vehicle groups (Fig. 6D). Relative *OCTN1* transcript abundance was also significantly greater after EGT than under either comparator condition (Control or Vehicle; Fig.

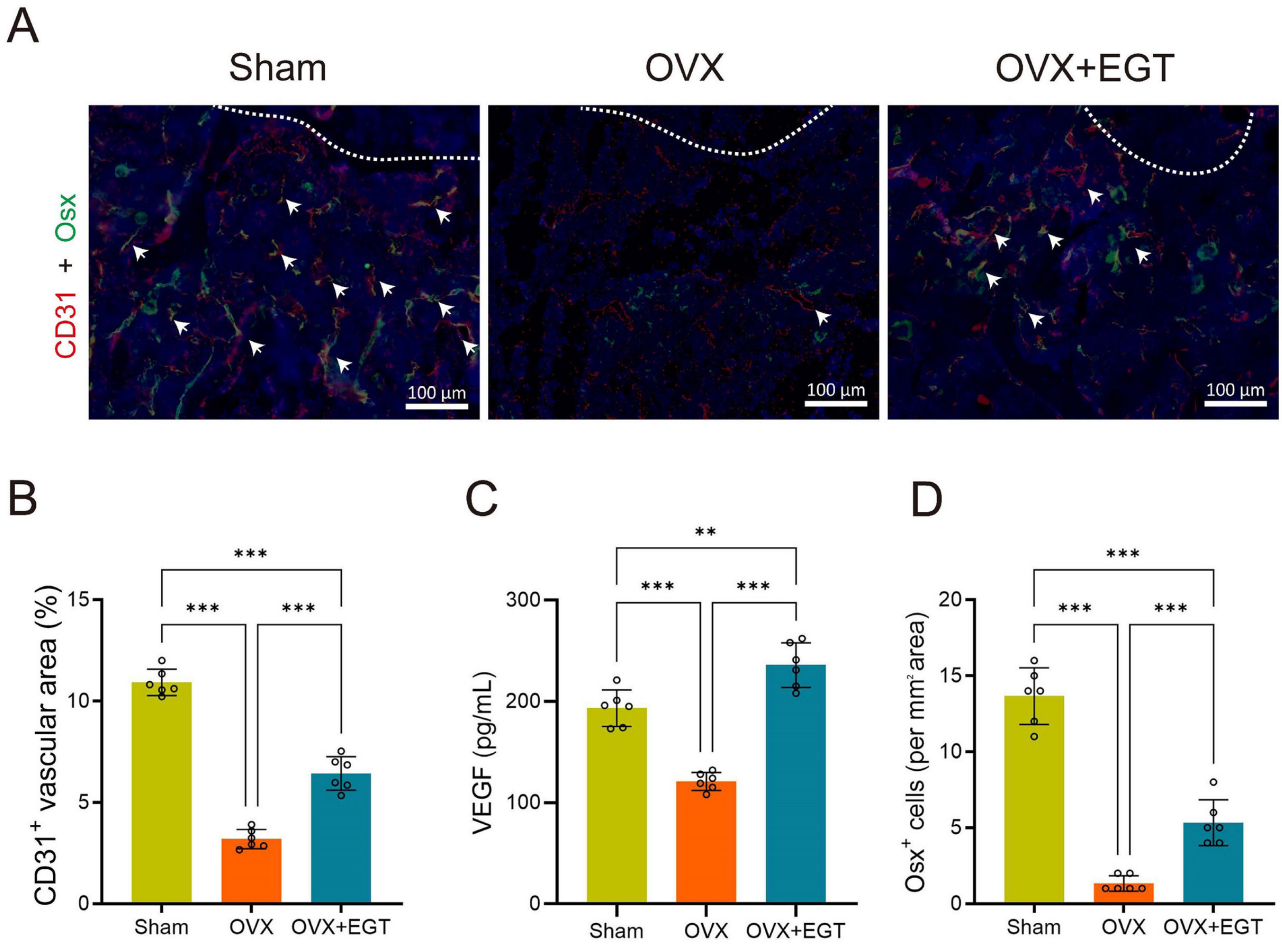

Fig. 5. EGT increases CD31$^+$ vascular area and Osx$^+$ osteogenic cell abundance and improves their spatial association in OVX mice. (A) Representative double immunofluorescence images of bone sections from the Sham, OVX, and OVX + EGT groups. CD31 was used to identify vascular endothelial structures, and Osx was used to identify osteogenic cells. White arrows indicate areas in which Osx$^+$ cells are located in close spatial proximity to CD31$^+$ vascular structures; scale bar: 100 μm. (B) Quantitative analysis of the CD31$^+$ vascular area in bone sections from the three groups. (C) Serum vascular endothelial growth factor (VEGF) levels in the three groups. (D) Quantification of the number of Osx$^+$ osteogenic cells in bone sections based on immunofluorescence images. Data are presented as the mean ± SD (n = 6 mice per group). $^{**}p < 0.01$, $^{***}p < 0.001$. The figure was created using Figdraw (https://www.figdraw.com/).

6E). Control and Vehicle cells formed relatively limited networks on Matrigel, whereas EGT-treated cells produced more extensive tube-like structures (Fig. 6F). Total tube length was significantly greater with EGT than under either comparator condition (Fig. 6G). These results show that EGT treatment increases OCTN1 expression and promotes angiogenesis in type H endothelial cells.

4. Discussion

PMOP is the most prevalent metabolic bone disorder associated with estrogen deficiency. Its hallmark pathological feature is disruption of bone metabolic homeostasis, primarily driven by estrogen deficiency-induced oxidative stress [7,33]. This disruption of bone remodeling contributes to progressive bone loss and greater susceptibility to fractures [34,35]. Studies have reported a substantial reduction in type H vessels in mouse models of OVX-induced bone loss [36,37]. These vessels are essential for maintaining bone homeostasis by coupling angiogenesis with osteogenesis [17,18]. We previously found that aging-associated oxidative stress promotes the accumulation of AOPPs, thereby contributing to the reduction of type H vessels in bone [19]. In this study, we found that EGT alleviated OVX-induced bone loss, reduced oxidative stress, and promoted angiogenesis by type H endothelial cells. The bone-protective effects of EGT may be associated with enhanced type H vessel–related angiogenesis.

Oxidative stress is an important component of estrogen deficiency-induced bone loss, affecting osteoclast formation, osteoblast differentiation, and osteocyte survival [34,35]. Guo et al. [26] showed that EGT reduced ROS accumulation and MAPK signaling in osteoclast precursors and preserved bone mass in OVX mice. More recently,

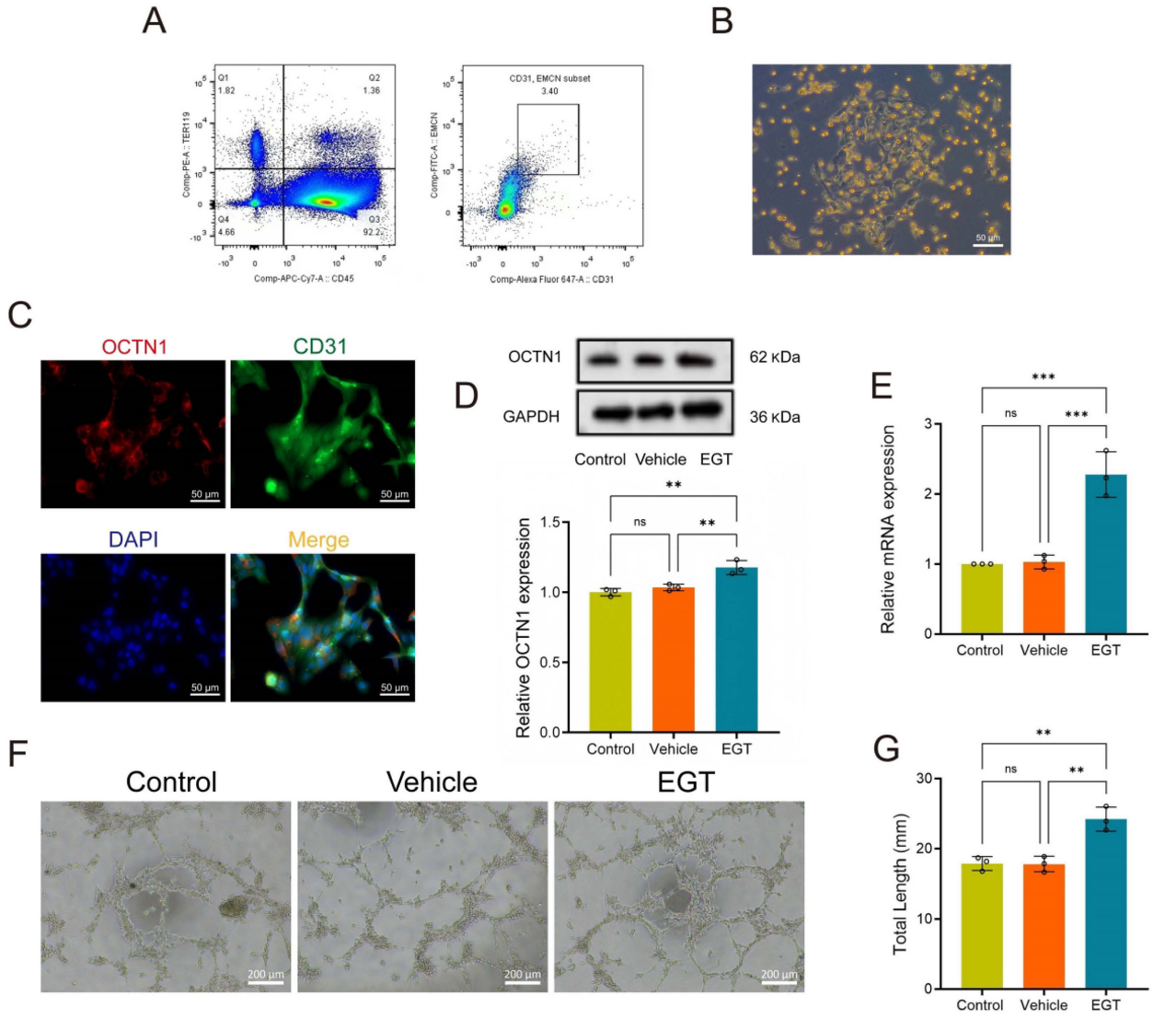

Fig. 6. EGT promotes angiogenesis in type H endothelial cells. (A) Flow cytometric identification and sorting of bone-derived $CD31^{+}EMCN^{+}$ endothelial cells. Bone marrow cells were first gated for the $CD45^{-}Ter119^{-}$ population to exclude hematopoietic and erythroid cells, followed by selection of the $CD31^{+}EMCN^{+}$ endothelial cell population. The boxed region indicates the sorted target cell population. (B) Representative bright-field image showing the morphology of primary cultured bone-derived $CD31^{+}EMCN^{+}$ endothelial cells; scale bar: 50 μm. (C) Representative immunofluorescence images showing OCTN1 expression in $CD31^{+}$ endothelial cells. OCTN1 is shown in red, CD31 in green, and nuclei stained with 4′,6-diamidino-2-phenylindole (DAPI) in blue. The merged image shows the overlay of the three fluorescence channels; scale bar: 50 μm. (D) Representative Western blot images and densitometric quantification of OCTN1 protein expression in the Control, Vehicle, and EGT groups. OCTN1 protein expression was normalized to GAPDH and expressed relative to the Control group. (E) Relative *OCTN1* mRNA expression normalized to *GAPDH* in the three groups. (F) Representative images of tube-like networks formed by endothelial cells on Matrigel in the Control, Vehicle, and EGT groups; scale bar: 200 μm. (G) Quantification of total tube length in the three groups. Data are presented as the mean ± SD from three independent experiments. $^{**}p < 0.01$, $^{***}p < 0.001$; ns, not significant. The figure was created using Figdraw (https://www.figdraw.com/).

Li et al. [27] reported that early EGT administration reduced mitochondrial ROS, inhibited NF-κB/NFATc1 signaling, and attenuated osteoclastogenesis and bone loss after OVX. A protective effect against oxidative mitochondrial injury has also been observed in chondrocytes [38]. In this study, EGT restored serum SOD activity and GSH levels while reducing serum concentrations of AOPPs and MDA. Micro-CT analysis demonstrated that EGT increased BMD and improved trabecular microarchitecture in OVX mice. These findings suggest that EGT may alleviate bone loss by enhancing antioxidant defenses and mitigating estrogen deficiency-induced oxidative damage.

Bone remodeling depends on the dynamic equilibrium between osteoclastic bone resorption and osteoblastic bone formation [39]. Our study found that EGT administration increased the bone formation markers OCN and P1NP while reducing the bone resorption markers TRAP, CTX-1, and NTX. These findings suggest that EGT restores the balance between bone formation and resorption in OVX mice. Histological analyses further showed that EGT reduced bone marrow adipocyte accumulation and enhanced osteoblastic OCN expression. Although previous studies have primarily emphasized the anti-resorptive effects of EGT through inhibition of osteoclastogenesis [26,27], our findings additionally indicate favorable effects on osteogenic activity.

The bone microvasculature is an essential component of the bone microenvironment that supports osteogenic activity and bone formation by supplying oxygen and nutrients and providing endothelial-derived angiocrine signals [40,41]. Our study found that EGT administration increased the $CD31^+$ vascular area and the number of Osx^+ osteogenic cells in bone tissue and enhanced their spatial co-localization. In addition, VEGF is an important component of the reciprocal signaling between osteogenic cells and the bone microvasculature [42]. It can promote angiogenesis and endothelial differentiation [43,44]. Serum VEGF levels were also significantly elevated following EGT administration. Our data indicate that EGT may enhance osteogenic activity by improving the bone microvasculature and strengthening its association with osteogenic cells.

Type H vessels represent a distinct subset of capillaries in bone and are essential for coupling angiogenesis with osteogenesis [17,18]. Type H endothelial cells support osteoprogenitor differentiation and bone formation through close spatial association and angiocrine signaling, particularly through Notch-dependent secretion of Noggin [18,45]. Conversely, osteogenic cells promote type H vessel formation by secreting angiogenic factors such as VEGF-A and SLIT3, thereby reinforcing angiogenesis–osteogenesis coupling [44,46]. Previous studies have shown that OCTN1 is the specific intracellular transporter responsible for EGT uptake [47,48]. In this study, we observed co-localization of OCTN1 with CD31, indicating that OCTN1 is expressed in type H endothelial cells. Moreover, EGT treatment upregulated OCTN1 expression in these cells and promoted angiogenesis. These results indicate that the pro-angiogenic effect of EGT on type H endothelial cells is associated with increased OCTN1 expression. EGT may enhance osteogenic activity and promote bone formation by promoting angiogenesis in type H endothelial cells.

Previous studies have shown that, following OCTN1-mediated uptake, EGT protects endothelial cells against oxidative injury by enhancing antioxidant enzyme activity, regulating GSH metabolism, and suppressing NOX1-mediated ROS production [49]. EGT also alleviates hyperglycemia-induced endothelial cytotoxicity and senescence by activating SIRT1 and SIRT6 and inhibiting p66Shc and NF-κB signaling, thereby reducing intracellular ROS levels [50]. Consistent with these antioxidant effects, our study showed that EGT enhanced enzymatic and non-enzymatic antioxidant defenses while reducing levels of oxidative damage products. Among these changes, the reduction in AOPPs may be particularly relevant to bone microvascular function, as our previous study demonstrated that AOPPs activated NOX-derived ROS, increased endothelial adhesion molecule expression, and impaired the proliferation, migration, and tube-forming activity of type H endothelial cells [19]. Taken together, EGT may promote bone formation and reduce bone loss by attenuating oxidative stress and enhancing type H vessel–related angiogenesis within the bone microvasculature.

However, several limitations should be acknowledged. First, because EGT administration was initiated 24 h after OVX, this study evaluated its preventive effects rather than its efficacy against established bone loss. Second, although EGT increased OCTN1 expression and enhanced tube formation in bone-derived $CD31^+EMCN^+$ endothelial cells, the causal role of OCTN1 was not established using knockdown, overexpression, or pharmacological inhibition. Third, because type H vessels were not identified by CD31/EMCN co-staining *in vivo*, the observed increase in $CD31^+$ vascular area cannot be interpreted as direct evidence of type H vessel formation. In addition, the increased spatial association between $CD31^+$ vessels and Osx^+ cells supports a closer vascular–osteogenic relationship but does not establish functional angiogenesis–osteogenesis coupling. Finally, the sample size of three mice per group used for H&E staining and OCN immunohistochemistry may limit statistical power and the precision of the corresponding estimates. Future studies using delayed EGT administration, OCTN1-targeted interventions, and direct structural and functional assessments of type H vessels are needed to clarify the underlying mechanism and determine whether EGT is effective against established osteoporosis.

5. Conclusion

In this study, early administration of EGT alleviated OVX-induced bone loss. This effect may be associated with reduced oxidative stress and enhanced type H vessel–related angiogenesis. As a naturally occurring rare amino acid with a favorable safety profile and excellent biocompatibility, EGT represents a promising candidate for the prevention of PMOP.

Availability of Data and Materials

No datasets requiring mandatory deposition, including sequence data, microarray data, genetic polymorphism data, macromolecular structure data, or crystallographic data, were generated or analyzed during the current study.

The datasets used and analyzed during the current study are available from the corresponding author on reasonable request.

Author Contributions

XPW conducted the experiments and wrote the manuscript; KZ and WYL conceived and designed the study; YZX performed data analysis; RWL and YCC prepared the figures. All authors contributed to editorial changes in the manuscript. All authors read and approved the final manuscript. All authors have participated sufficiently in the work and agreed to be accountable for all aspects of the work.

Ethics Approval and Consent to Participate

All surgical interventions, treatments, and postoperative animal care procedures were strictly carried out in accordance with the "Guidelines for the Care and Use of Laboratory Animals of the National Institutes of Health" and were approved by the Experimental Animal Care and Use Committee of the First Affiliated Hospital of Gannan Medical University (No. GMU2022126). The study followed the ARRIVE guidelines.

Acknowledgment

We thank Figdraw (https://www.figdraw.com/) for providing the drawing materials/templates used in the preparation of the graphical abstract.

Funding

This work was supported by the Jiangxi Provincial Natural Science Foundation (No.20252BAC200539), the Technology Project of Health Commission of Jiangxi Province (No.202510464), and the Technology Project of Ganzhou (No.GZ2024YLJ129).

Conflicts of Interest

The authors declare no conflicts of interest.

Declaration of AI and AI-Assisted Technologies in the Writing Process

We used ChatGPT software to improve our English. The authors checked the article, made appropriate revisions, and are responsible for the article.

Supplementary Material

Supplementary material associated with this article can be found, in the online version, at https://doi.org/10.31083/FBL54657.

References

[1] Reid IR, Bolland MJ. Management of postmenopausal osteoporosis. Endocrine Reviews. 2026; 47: 468–495. https://doi.org/10.1210/endrev/bnag006

[2] Eastell R, O'Neill TW, Hofbauer LC, Langdahl B, Reid IR, Gold DT, et al. Postmenopausal osteoporosis. Nature Reviews. Disease Primers. 2016; 2: 16069. https://doi.org/10.1038/nrdp.2016.69

[3] Wang L, Yu W, Yin X, Cui L, Tang S, Jiang N, et al. Prevalence of Osteoporosis and Fracture in China: The China Osteoporosis Prevalence Study. JAMA Network Open. 2021; 4: e2121106. https://doi.org/10.1001/jamanetworkopen.2021.21106

[4] Willers C, Norton N, Harvey NC, Jacobson T, Johansson H, Lorentzon M, et al. Osteoporosis in Europe: a compendium of country-specific reports. Archives of Osteoporosis. 2022; 17: 23. https://doi.org/10.1007/s11657-021-00969-8

[5] GBD 2019 Fracture Collaborators. Global, regional, and national burden of bone fractures in 204 countries and territories, 1990-2019: a systematic analysis from the Global Burden of Disease Study 2019. The Lancet. Healthy Longevity. 2021; 2: e580–e592. https://doi.org/10.1016/S2666-7568(21)00172-0

[6] Weitzmann MN, Pacifici R. Estrogen deficiency and bone loss: an inflammatory tale. The Journal of Clinical Investigation. 2006; 116: 1186–1194. https://doi.org/10.1172/JCI28550

[7] Manolagas SC. From estrogen-centric to aging and oxidative stress: a revised perspective of the pathogenesis of osteoporosis. Endocrine Reviews. 2010; 31: 266–300. https://doi.org/10.1210/er.2009-0024

[8] Sies H. Oxidative Stress: Concept and Some Practical Aspects. Antioxidants (Basel, Switzerland). 2020; 9: 852. https://doi.org/10.3390/antiox9090852

[9] Sies H, Jones DP. Reactive oxygen species (ROS) as pleiotropic physiological signalling agents. Nature Reviews. Molecular Cell Biology. 2020; 21: 363–383. https://doi.org/10.1038/s41580-020-0230-3

[10] Valko M, Leibfritz D, Moncol J, Cronin MTD, Mazur M, Telser J. Free radicals and antioxidants in normal physiological functions and human disease. The International Journal of Biochemistry & Cell Biology. 2007; 39: 44–84. https://doi.org/10.1016/j.biocel.2006.07.001

[11] Marcucci G, Domazetovic V, Nediani C, Ruzzolini J, Favre C, Brandi ML. Oxidative Stress and Natural Antioxidants in Osteoporosis: Novel Preventive and Therapeutic Approaches. Antioxidants (Basel, Switzerland). 2023; 12: 373. https://doi.org/10.3390/antiox12020373

[12] Vijayan V, Khandelwal M, Manglani K, Singh RR, Gupta S, Surolia A. Homocysteine alters the osteoprotegerin/RANKL system in the osteoblast to promote bone loss: pivotal role of the redox regulator forkhead O1. Free Radical Biology & Medicine. 2013; 61: 72–84. https://doi.org/10.1016/j.freeradbiomed.2013.03.004

[13] Baek KH, Oh KW, Lee WY, Lee SS, Kim MK, Kwon HS, et al. Association of oxidative stress with postmenopausal osteoporosis and the effects of hydrogen peroxide on osteoclast formation in human bone marrow cell cultures. Calcified Tissue International. 2010; 87: 226–235. https://doi.org/10.1007/s00223-010-9393-9

[14] Bai XC, Lu D, Bai J, Zheng H, Ke ZY, Li XM, et al. Oxidative stress inhibits osteoblastic differentiation of bone cells by ERK and NF-kappaB. Biochemical and Biophysical Research Communications. 2004; 314: 197–207. https://doi.org/10.1016/j.bbrc.2003.12.073

[15] Ran D, Zhou D, Liu G, Ma Y, Ali W, Yu R, et al. Reactive Oxygen Species Control Osteoblast Apoptosis through SIRT1/PGC-1α/P53^{Lys382} Signaling, Mediating the Onset of Cd-Induced Osteoporosis. Journal of Agricultural and Food Chemistry. 2023; 71: 5991–6002. https://doi.org/10.1021/acs.jafc.2c08505

[16] Jilka RL, Weinstein RS, Parfitt AM, Manolagas SC. Quantifying osteoblast and osteocyte apoptosis: challenges and rewards. Journal of Bone and Mineral Research : the Official Journal of

the American Society for Bone and Mineral Research. 2007; 22: 1492–1501. https://doi.org/10.1359/jbmr.070518
[17] Peng Y, Wu S, Li Y, Crane JL. Type H blood vessels in bone modeling and remodeling. Theranostics. 2020; 10: 426–436. https://doi.org/10.7150/thno.34126
[18] Kusumbe AP, Ramasamy SK, Adams RH. Coupling of angiogenesis and osteogenesis by a specific vessel subtype in bone. Nature. 2014; 507: 323–328. https://doi.org/10.1038/nature13145
[19] Zhao K, Zhu GZ, Li HZ, Gao JW, Tu C, Wu DZ, et al. Accumulation of Advanced Oxidation Protein Products Promotes Age-Related Decline of Type H Vessels in Bone. The Journals of Gerontology. Series A, Biological Sciences and Medical Sciences. 2024; 80: glae271. https://doi.org/10.1093/gerona/glae271
[20] Kim D, Piao J, Park JS, Lee D, Hwang DY, Hong HS. Substance P-Mediated Vascular Protection Ameliorates Bone Loss. Oxidative Medicine and Cellular Longevity. 2023; 2023: 9903336. https://doi.org/10.1155/2023/9903336
[21] Liu HM, Tang W, Wang XY, Jiang JJ, Zhang W, Wang W. Safe and Effective Antioxidant: The Biological Mechanism and Potential Pathways of Ergothioneine in the Skin. Molecules (Basel, Switzerland). 2023; 28: 1648. https://doi.org/10.3390/molecules28041648
[22] Apparoo Y, Phan CW, Kuppusamy UR, Sabaratnam V. Ergothioneine and its prospects as an anti-ageing compound. Experimental Gerontology. 2022; 170: 111982. https://doi.org/10.1016/j.exger.2022.111982
[23] Cumming BM, Chinta KC, Reddy VP, Steyn AJC. Role of Ergothioneine in Microbial Physiology and Pathogenesis. Antioxidants & Redox Signaling. 2018; 28: 431–444. https://doi.org/10.1089/ars.2017.7300
[24] Paul BD. Ergothioneine: A Stress Vitamin with Antiaging, Vascular, and Neuroprotective Roles? Antioxidants & Redox Signaling. 2022; 36: 1306–1317. https://doi.org/10.1089/ars.2021.0043
[25] Borodina I, Kenny LC, McCarthy CM, Paramasivan K, Pretorius E, Roberts TJ, et al. The biology of ergothioneine, an antioxidant nutraceutical. Nutrition Research Reviews. 2020; 33: 190–217. https://doi.org/10.1017/S0954422419000301
[26] Guo Z, Huang Y, Wang X, Han Y, Li A, Qu Y, et al. Ergothioneine alleviates osteoporosis via the ROS-MAPK signaling Axis. Bone. 2025; 197: 117496. https://doi.org/10.1016/j.bone.2025.117496
[27] Li G, Fang Q, Lin Z, Zhang C, Gao C, Zhu D, et al. Ergothioneine prevents ovariectomy-induced osteoporosis by suppressing NF-κB/p65 signalling to attenuate osteoclastogenesis and bone marrow inflammation. Bone & Joint Research. 2026; 15: 248–263. https://doi.org/10.1302/2046-3758.153.BJR-2025-0316.R2
[28] Tang RMY, Cheah IKM, Yew TSK, Halliwell B. Distribution and accumulation of dietary ergothioneine and its metabolites in mouse tissues. Scientific Reports. 2018; 8: 1601. https://doi.org/10.1038/s41598-018-20021-z
[29] Batoon L, Millard SM, Raggatt LJ, Wu AC, Kaur S, Sun LWH, et al. Osteal macrophages support osteoclast-mediated resorption and contribute to bone pathology in a postmenopausal osteoporosis mouse model. Journal of Bone and Mineral Research : the Official Journal of the American Society for Bone and Mineral Research. 2021; 36: 2214–2228. https://doi.org/10.1002/jbmr.4413
[30] Luengo-Mateos M, González-Vila A, Torres Caldas AM, Alasaoufi AM, González-Domínguez M, López M, et al. Protocol for ovariectomy and estradiol replacement in mice. STAR Protocols. 2024; 5: 102910. https://doi.org/10.1016/j.xpro.2024.102910
[31] Martin KR. The bioactive agent ergothioneine, a key component of dietary mushrooms, inhibits monocyte binding to endothelial cells characteristic of early cardiovascular disease. Journal of Medicinal Food. 2010; 13: 1340–1346. https://doi.org/10.1089/jmf.2009.0194
[32] Chen JK, Deng YP, Jiang GJ, Liu YZ, Zhao T, Shen FM. Establishment of tube formation assay of bone marrow-derived endothelial progenitor cells. CNS Neuroscience & Therapeutics. 2013; 19: 533–535. https://doi.org/10.1111/cns.12102
[33] Lean JM, Davies JT, Fuller K, Jagger CJ, Kirstein B, Partington GA, et al. A crucial role for thiol antioxidants in estrogen-deficiency bone loss. The Journal of Clinical Investigation. 2003; 112: 915–923. https://doi.org/10.1172/JCI18859
[34] Mohamad NV, Ima-Nirwana S, Chin KY. Are Oxidative Stress and Inflammation Mediators of Bone Loss Due to Estrogen Deficiency? A Review of Current Evidence. Endocrine, Metabolic & Immune Disorders Drug Targets. 2020; 20: 1478–1487. https://doi.org/10.2174/1871530320666200604160614
[35] Lean JM, Jagger CJ, Kirstein B, Fuller K, Chambers TJ. Hydrogen peroxide is essential for estrogen-deficiency bone loss and osteoclast formation. Endocrinology. 2005; 146: 728–735. https://doi.org/10.1210/en.2004-1021
[36] Huang J, Yin H, Rao SS, Xie PL, Cao X, Rao T, et al. Harmine enhances type H vessel formation and prevents bone loss in ovariectomized mice. Theranostics. 2018; 8: 2435–2446. https://doi.org/10.7150/thno.22144
[37] Jia J, He R, Yao Z, Su J, Deng S, Chen K, et al. Daidzein alleviates osteoporosis by promoting osteogenesis and angiogenesis coupling. PeerJ. 2023; 11: e16121. https://doi.org/10.7717/peerj.16121
[38] Sakata S, Kunimatsu R, Tanimoto K. Protective Effect of Ergothioneine against Oxidative Stress-Induced Chondrocyte Death. Antioxidants (Basel, Switzerland). 2024; 13: 800. https://doi.org/10.3390/antiox13070800
[39] Raggatt LJ, Partridge NC. Cellular and molecular mechanisms of bone remodeling. The Journal of Biological Chemistry. 2010; 285: 25103–25108. https://doi.org/10.1074/jbc.R109.041087
[40] Sivan U, De Angelis J, Kusumbe AP. Role of angiocrine signals in bone development, homeostasis and disease. Open Biology. 2019; 9: 190144. https://doi.org/10.1098/rsob.190144
[41] Chen J, Hendriks M, Chatzis A, Ramasamy SK, Kusumbe AP. Bone Vasculature and Bone Marrow Vascular Niches in Health and Disease. Journal of Bone and Mineral Research : the Official Journal of the American Society for Bone and Mineral Research. 2020; 35: 2103–2120. https://doi.org/10.1002/jbmr.4171
[42] Long F, Li H, Chen X, He Y, Dong Y. Exosomal miR-423-5p Derived from Mineralized Osteoblasts Promotes Angiogenesis of Endothelial Cells by Targeting CXCL10. Frontiers in Bioscience (Landmark Edition). 2024; 29: 278. https://doi.org/10.31083/j.fbl2908278
[43] Ribatti D, d'Amati A. Bone angiocrine factors. Frontiers in Cell and Developmental Biology. 2023; 11: 1244372. https://doi.org/10.3389/fcell.2023.1244372
[44] Wille A, Weske S, von Wnuck Lipinski K, Wollnitzke P, Schröder NH, Thomas N, et al. Sphingosine-1-phosphate promotes osteogenesis by stimulating osteoblast growth and neovascularization in a vascular endothelial growth factor-dependent manner. Journal of Bone and Mineral Research : the Official Journal of the American Society for Bone and Mineral Research. 2024; 39: 357–372. https://doi.org/10.1093/jbmr/zjae006
[45] Ramasamy SK, Kusumbe AP, Wang L, Adams RH. Endothelial Notch activity promotes angiogenesis and osteogenesis in bone. Nature. 2014; 507: 376–380. https://doi.org/10.1038/nature13146
[46] Xu R, Yallowitz A, Qin A, Wu Z, Shin DY, Kim JM, et al.

Targeting skeletal endothelium to ameliorate bone loss. Nature Medicine. 2018; 24: 823–833. https://doi.org/10.1038/s41591-018-0020-z

[47] Gründemann D, Harlfinger S, Golz S, Geerts A, Lazar A, Berkels R, et al. Discovery of the ergothioneine transporter. Proceedings of the National Academy of Sciences of the United States of America. 2005; 102: 5256–5261. https://doi.org/10.1073/pnas.0408624102

[48] Gründemann D, Hartmann L, Flögel S. The ergothioneine transporter (ETT): substrates and locations, an inventory. FEBS Letters. 2022; 596: 1252–1269. https://doi.org/10.1002/1873-3468.14269

[49] Li RWS, Yang C, Sit ASM, Kwan YW, Lee SMY, Hoi MPM, et al. Uptake and protective effects of ergothioneine in human endothelial cells. The Journal of Pharmacology and Experimental Therapeutics. 2014; 350: 691–700. https://doi.org/10.1124/jpet.114.214049

[50] D'Onofrio N, Servillo L, Giovane A, Casale R, Vitiello M, Marfella R, et al. Ergothioneine oxidation in the protection against high-glucose induced endothelial senescence: Involvement of SIRT1 and SIRT6. Free Radical Biology & Medicine. 2016; 96: 211–222. https://doi.org/10.1016/j.freeradbiomed.2016.04.013